Carro, G., …et al. (2014) Fabrication and characterization of Y2O3 dispersion strengthened copper alloys. *Journal of Nuclear Materials*, 455(1-3), pp.: 655-659.

DOI: https://doi.org/10.1016/j.jnucmat.2014.08.050

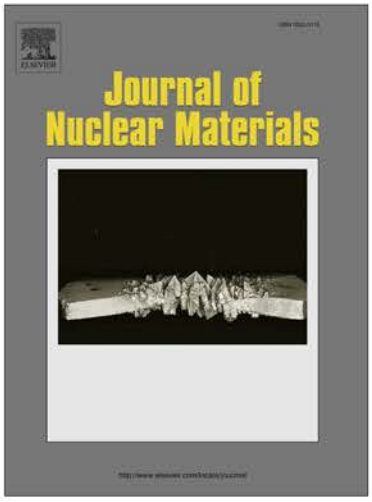

Fabrication and characterization of Y_2O_3 dispersion strengthened copper alloys

G. Carro, A. Muñoz, M.A. Monge, B. Savoini, R. Pareja, C. Ballesteros, P. Adeva

PII: S0022-3115(14)00578-9
DOI: http://dx.doi.org/10.1016/j.jnucmat.2014.08.050
Reference: NUMA 48401

To appear in: *Journal of Nuclear Materials*

Please cite this article as: G. Carro, A. Muñoz, M.A. Monge, B. Savoini, R. Pareja, C. Ballesteros, P. Adeva, Fabrication and characterization of Y_2O_3 dispersion strengthened copper alloys, *Journal of Nuclear Materials* (2014), doi: http://dx.doi.org/10.1016/j.jnucmat.2014.08.050

FABRICATION AND CHARACTERIZATION OF Y_2O_3 DISPERSION STRENGTHENED COPPER ALLOYS

G. Carro[1], A. Muñoz[1], M.A. Monge[1*], B. Savoini[1], R. Pareja[1], C. Ballesteros[1] and P. Adeva[2]

[1*]*Departamento de Física, Universidad Carlos III de Madrid, 28911 Leganés, Spain*

[2]*Centro Nacional de Investigaciones Metalúrgicas, CSIC, Av. Gregorio del Amo, 8, 28040 Madrid, Spain*

ABSTRACT

Three cooper base materials were fabricated following different routes: cast Cu-1wt.%Y (C-Cu1Y) produced by vacuum induction melting, and Cu-1wt.%Y (PM-Cu1Y) and Cu-1wt.%Y_2O_3 (PM-Cu1Y_2O_3) both processed by a powder metallurgy route and sintering by hot isostatic pressing. PM-Cu1Y alloy was prepared by cryomilling and PM-Cu1Y_2O_3 by conventional milling at room temperature. The materials were characterized by X-ray diffraction, optical and electron microscopy and microhardness measurements. C-Cu1Y presents a characteristic eutectic microstructure while PM-Cu1Y_2O_3 exhibits a composite like microstructure. Electron microscopy analyses of as-HIP PM-Cu1Y revealed irregular decoration of yttrium-rich oxides at the grain boundaries and an inhomogeneous dispersion of polygonal shaped yttrium-rich oxides dispersed in the Cu matrix. Tensile tests performed on PM-Cu-1Y on the temperature range of 293 K – 773 K have showed a decrease of the yield strength at temperatures higher than 473 K, and monotonically decrease of the ultimate tensile strength and maximum plastic strain on increasing temperature.

Keywords

Oxide Dispersion Strengthened materials, Cu alloys, Powder metallurgy, Cryomilling, Mechanical properties.

[*]**Corresponding author:**

E-mail address: mmonge@fis.uc3m.es

1. Introduction

Pure copper is an important technological material due to its high electrical and thermal conductivities. However, the use of pure copper as structural material for high heat flux applications in the range 373-673 K, is often limited because of its low strength at relatively high temperatures. In the last years a lot of works have been carried out in copper-based materials in order to find an optimal combination of high mechanical strength and high thermal conductivity [1-7]. A comprehensive review of copper based materials for applications in fusion energy systems can be found in Ref. [4-7] and references therein. Various mechanisms to achieve long-term high-temperature strength in copper alloys have been considered, such as alloying and dispersion of fine hard particles [8-14]. CuCrZr alloy has higher strength than pure copper at room temperature but at high temperature the decomposition of the supersaturated solid solution in the alloy originates a degradation of its mechanical properties. In spite of this, CuCrZr has been chosen as the reference material for the water cooling system of ITER, with an operating temperature in the range 523-598 K [8, 15-19]. Cold working and precipitation hardening are strengthening methods not applicable for materials operating at high temperature due to the detrimental effects of recrystallization, dissolution and particle coarsening on the mechanical properties. In order to raise the operating temperature, copper base materials strengthened by dispersion of hard particles, as for instance Y_2O_3 or Al_2O_3, have been considered [20-22]. the low influence of dispersoids on the thermal conductivity of the matrix favors the use of this strengthening mechanism compared with solid solution hardening, which significantly lowers the thermal conductivity of copper.

Different techniques can be used for incorporating oxide hard particles, such as internal oxidation, surface oxidation, mechanical milling and gel precipitation. In this work

different routes have been explored in order to produce oxide dispersion strengthened (ODS) copper with a dispersion of stable yttrium-rich oxide nanoparticles, mainly Y_2O_3. The microstructure of the different ODS copper materials has been analyzed and the mechanical properties of the material with the most promising microstructure and fine dispersion of reinforcing particles have been studied.

2. Experimental

Three copper-yttrium based materials have been prepared following three fabrication routes. The starting materials were ingots of pure Cu and Y supplied by Alpha-Aesar, and Cu, Y and Y_2O_3 powders with purity and mean particle size of 99.995% and 37 μm, 99.98% and 420 μm, and 99.9% and 25 nm, respectively. One ingot with the composition of Cu-1wt.%Y (labeled as C-Cu1Y) was produced by vacuum induction melting and casting into a graphite crucible. Powder blends with the following target compositions: Cu-1wt.%Y (PM-Cu1Y) and Cu-1wt.%Y_2O_3 (PM-CuY_2O_3) were prepared mixing the powders in a turbula shaker-mixer for 4 h at 95 r.p.m. to attain homogenous blends. The PM-Cu1Y blend was cryomilled for 1 h at 320 rpm in a vertical attritor using liquid nitrogen as cryogenic fluid, and 5 mm ∅Cr-Steel balls as grinding media with a ball-powder ratio of 9:1. The PM-CuY_2O_3 blend was mechanically for 10 h at room temperature in a high-energy planetary at 100 rpm under a high purity Ar atmosphere using 10 mm ∅Cr-Steel balls with a ball-powder ratio of 9:1. Milling rate at higher rpm caused the formation of Cu pellets with a size of ≈1 cm by cold welding. PM-Cu1Y and PM-CuY_2O_3 powders were canned in steel containers, degassed at 573 K for 24 h in vacuum, vacuum sealed, and sintered by hot isostatic

pressing (HIP) at 1083 K for 2 h at a pressure of 172 MPa. The powders were handled throughout the process under a high purity Ar atmosphere using a glove box.

The microstructural characteristics of the materials were investigated using optical microscopy, scanning electron microscopy (SEM), transmission electron microscopy (TEM), energy-dispersive X-ray spectroscopy (EDS) analyses and X-ray diffraction (XRD) analyses. The density of the sintered materials was measured using a He ultrapycnometer. Vickers microhardness measurements were performed applying a load of 2.94 N for 20 s, and tensile-tests were performed in the temperature range of 293 to 723 K at a strain rate of 1.1×10^{-4} s^{-1} on tensile specimens with 15 mm gauge length ×6 mm width ×1 mm thickness. A minimum of three specimens were tested at each temperature in order to verify the reproducibility of the measurements and estimate the uncertainties. The tensile tests above room temperature were done under a protective atmosphere of flowing argon.

3. Results and discussion

3.1 Microstructure

C-C*u*1Y

Figs. 1a-b) shows the microstructure of a C-Cu1Y sample in the as-cast condition. It presents the characteristic microstructure of a eutectic alloy containing separate and distinct solid phases, with formation of complex eutectic substructures at the Cu grain boundaries [23]. Fig. 1c) shows EDS analyses from different eutectic substructures. These results reveal that these substructures have diverse yttrium content. XRD measurements (Fig. 2a) have confirmed the presence of the Cu_2Y and CuY eutectic compounds. Nevertheless, peaks attributed to Y_2O_3 were detected in the XRD patterns.

According to the Cu-Y phase diagram, the presence of other eutectic compounds as Cu_4Y and Cu_7Y_2 should not be discarded [23]. These hard and brittle Y-Cu intermetallic compounds promote the formation of microcraks due to fast cooling during casting as the inset in Fig. 1b) reveals. The density, grain size and microrhardness values are given in Table 1. The low density of this alloy appears to be due to the presence, although scantly, of spherical macrocavities. The mean grain size of 20±4 μm and the microhardness value of 680 MPa were found.

PM-C*u*1Y

The XRD patterns from the milled powder and consolidated alloy are depicted in Fig. 2b). In the milled power pattern, a peak corresponding to Y_2O_3 is clearly visible that confirm the formation of the oxide during the cryomilling of the blend of copper and yttrium powders. The crystallite sizes in the milled powder, calculated by the Williamson-Hall analysis [24], resulted in a crystallite average size of ~35 nm. No peak associated with Y_2O_3 or other compound is observed in the XRD pattern of the consolidated material indicating that Y content should be dispersed throughout the sample.

Fig. 3a) shows an optical microscopy image of the consolidated PM-Cu1Y. The mean grain size is 8±2 μm, the relative density is 99% and the microhardness value 712 MPa. The inset in Fig. 3a) shows a BSE-SEM- image of a small area. Submicrometer particles, with sizes < 0.5 μm (dark regions) are found decorating the grain boundaries. EDS analyses indicated that these particles are yttrium-rich oxides. Neither microcavities nor voids have been observed.

TEM observations revealed the presence of yttrium-rich oxide particles dispersed inside the Cu grains with sizes ranging from ~25 nm to 95 nm as Fig. 3b) illustrates. These

particles exhibit a characteristic polygonal shape and are inhomogeneously distributed, forming aggregates in some cases. Not coherence of the oxide particles with the matrix was observed.

PM-C*u*1Y_2O_3

The XRD patterns from the milled powder and consolidated material are represented in Fig. 2c). It should be noted the presence of Y_2O_3 in both cases. Optical and SEM microscopy images of the consolidated material are depicted on Fig. 4a). The material presents a composite-like microstructure with aggregates of spherical Y_2O_3 particles embedded in the interstices between the powder particles. Fig. 4b) shows a TEM image of one of these Y_2O_3 aggregates . Also, some nanoparticles with a mean size of ~30 nm are observed inside the copper grains, see Fig. 4c). EDS analysis reveals that these nanoparticles are Y-oxide indicating that a oxide dispersion could be achieved by the present route.

The consolidated material is fully dense and has a microhardness of 620 MPa and with mean grain size of 16 ±3 μm, that is twice the corresponding to PM-Cu1Y. This indicates that an effective dispersion of Y_2O_3 to restrain grain growth during the HIP process has not been achieved, probably due to the milling conditions. Cu is a very ductile material and cold welding of copper particles due to collision with ball media appears to prevent a fine dispersion of the oxide particles in a Cu matrix.

3.2 Tensile tests

Considering the previous results, tensile tests were performed on the PM-Cu1Y alloy. Compared with other materials, this alloy exhibits dispersion of oxide nanoparticles inside the copper grains, as well as the lowest grain size and higher microhardness. Fig. 5 shows the true stress-strain curves for PM-Cu1Y at temperatures ranging from 293 to 773 K. The tensile characteristics are summarized in Table 2. The yield strength (YS) and ultimate tensile strength (UTS) decrease with temperature. A lineal decrease of the UTS at a rate of -0.48±0.03 $MPaK^{-1}$ is found, see inset on Fig. 5. The strain hardening ratio, defined as the ratio of the UTS to the YS, undergoes a continuous reduction increasing temperature from 2.4 ± 0.3 at 293 K to 1.18 ± 0.10 at 773 K. This ratio is an indicator of the amount of strain hardening that a material can suffer during deformation.

Another remarkably feature in the tensile curves is the anomalous behavior of the maximum plastic strain with temperature, which decreases from a value of 26 ± 3 % at 293 K to 9.9 ± 0.8 % at 773 K.

The YS of the PM-Cu1Y alloy is higher than that reported for oxygen-free high-conductivity (OFHC) Cu [4]. The yield strength of PM-Cu1Y improves the corresponding value for OFHC Cu in a factor of ~2 at 293 K and ~4.2 at 573 K. This enhancement appears to be associated with to Y-oxide reinforcement [20]. However, the precipitation hardened CuCrZr alloy, which is considered in ITER for various critical applications, exhibits better mechanical properties than the studied Cu-Y alloy. The reported values of YS and UTS for CuCrZr alloy (0.6-0.9 wt% Cr and 0.07-0.15 wt% Zr) after solution annealing and ageing are 288 and 400 MPa at 293 K and 182 and 205 MPa at 773 K, respectively [8,16].

Figs. 6 a) and b) show SEM images of The fracture surfaces of samples tested at room temperature. The surfaces display small and poorly defined quasi-cleavage facets, connected by shallow dimples, see Fig. 6. The images also reveal that large dimples are associated with yttrium-rich oxides mainly present at the grain boundaries. These characteristics correspond to a typical semi-brittle fracture surface consisting of small cleavage facets linked by ductile ridges covered by dimples. As the temperature increases, the dimples become randomly distributed, almost covering the entire fracture surface, as is shown in Fig. 6 c) and d) for samples tested at 573 K. Furthermore, the dimples size significantly increases in comparison with those formed at lower temperatures, and larger cavities develop by coalescence of microvoids. At temperatures higher than 573 K the growth of a thin oxide layer hinders the fracture surface, although the increase of the size of the dimples and their homogenous distribution is still visible.

The numerous yttrium-rich oxide particles observed on the dimples surface indicate that the dimples were formed by a boundary decohesion process. In ductile materials, dimples develop with a characteristic shear-lip structure. However, in PM-Cu1Y this structure is not well developed under the present conditions. Both features indicate that the plasticity of the material is quite limited besides the increase of the dimple size with temperature induced by grain boundary decohesion. This decohesion can be favored by the Y-oxide.

4. Conclusions

Three different routes were explored to fabricate ODS copper alloys: vacuum induction melting and casting (C-Cu1Y), cryomilling (PM-Cu1Y), or mechanical alloying at RT (PM-CuY_2O_3), following by HIP consolidation. PM-Cu1Y compared with the other

alloys presents a significant dispersion of oxide nanoparticles inside the copper grains, the lowest grain size and highest microhardness. These results indicate that the cryomilling can be an effective processing route to obtain a fully dense material with a promising microstructure for improving The mechanical properties of Cu base alloys.

The tensile properties of PM-Cu1Y have been studied at constant strain rate in the temperature range 293-773 K. This alloy exhibits enhanced mechanical properties compared to OFHC Cu which are attributed to the presence of reinforcement yttrium-rich oxide particles.

In order to attain ODS Cu base material suitable to operate at elevated temperature, further efforts to obtain an effective homogeneous Y-oxide dispersion avoiding the grain boundaries decoration with Y-oxide agglomerates are required.

Acknowledgements

This research has been supported by Ministerio de Economía y Competitividad of Spain (ENE2012-39787-C06-05). The financial support from the Comunidad de Madrid, through the programs TECHNOFUSION (S2009/ENE-1679) and ESTRUMAT (CM S2009MAT-1585), and the additional subvention from EURATOM/CIEMAT association through contract EFDA (WP12-MAT-HHFMAM-02) are also gratefully acknowledged.

References

[1] M. Al-Hajri, A. Melendez, R. Woods, T.S. Srivatsan, J. Alloy. Compd. 290 (1999) 290–297.

[2] M.A. Atwater, D. Roy , K.A. Darling, B. G. Butler, R.O. Scattergood, C.C. Koch, Mat. Sci. Eng. A-Struct. 558 (2012) 226–233.

[3] E. Botcharova, M. Heilmaier, J. Freudenberger, G. Drew, D. Kudashow, U. Martin, L. Schultz, J. Alloy. Compd. 351 (2003) 119–125.

[4] M. Li, S.J. Zinkle , in "*Comprehensive Nuclear Materials"*, R.J.M. Konings (Ed.), Elsevier (Amsterdam) vol. 4 (2012) 667-690.

[5] J.H. You, H. Bolt, J. Nucl. Mater. 307–311 (2002) 74–78.

[6] K.D. Leedy, J.F. Stubbins, Mat. Sci. Eng. A-Struct. 297 (1-2) (2001) 10–18.

[7] S.A. Fabritsiev, S.J. Zinkle, B.N. Singh, J. Nucl. Mater. 233-237 (1996) 127-137.

[8] V.R. Barabash, G.M. Kalinin, S.A. Fabritsiev, S.J. Zinkle, J. Nucl. Mater. 417 (2011) 904-907.

[9] M. Li, J.K. Heuer, J.F Stubbins, D.J. Edwards, J. Nucl. Mater. 283–287 (2) (2000), 977-981.

[10] J.R. Groza, J.C. Gibeling, Mat. Sci. Eng. A-Struct. 171 (1–2) (1993) 115–125.

[11] J. Groza, J. Mater. Eng. Perform. 1 (1) (1992) 113-121.

[12] J.A. Rogers, Powder Metall. 20 (4) (1977) 212-220.

[13] N. Fuschillo, M.L. Gimpl, J. Met. 23 (1971) 43-45.

[14] W.F. Schilling, N.J. Grant, Metall. Trans. 1 (8), (1970) 2205-2210.

[15] C. Rotti, N. Panda, H. Patel, N. Kanoongo, A. Chakraborty, K. Balasubramanian, Fusion Sci. Technol. 65 (2) (2014) 205-211.

[16] V.R. Barabash, The ITER International Team, A. Peacock, S. Fabritsiev,

G. Kalinin, S. Zinkle, A. Rowcliffe, J.-W. Rensman, A.A. Tavassoli,

P. Marmy, P.J. Karditsas, F. Gillemot, M. Akiba, J. Nucl. Mater. 367–370 (2007) 21–32

[17] R. Andreani, M. Gasparotto, Fusion Eng. Des. 61/62 (2004) 27-36.

[18] H. Bolt, V. Barabash, G. Federici, J. Linke, A. Loarte, J. Roth, K. Sato, J. Nucl. Mater. 307–311 (2002) 43–52.

[19] S. Majumdar, G. Kalinin, J. Nucl. Mater. 283–287 (2000) 1424-1428.

[20] D.V. Kudashov, H. Baum, U. Martin, M. Heilmaier, H. Oettel, Materials Science and Engineering A 387-389 (2004) 768-771.

[21] X. Wang, S. Liang, P. Yang. Z. Fan, J. Mater. Eng. Perform. 19 (2010) 1330-1336.

[22] M.N. Avettand-Fènoël, A. Simar, R. Shabadi, R. Taillard, B. de Messter, Mater. Design 60 (2014) 343-357.

[23] H. Okamoto, Journal of Phase Equilibria 13(1) (1992) 102-103.

[24] G.K. Williamson, W.H. Hall, Acta Metall. 1 (1953) 22-31.

Tables:

Table 1: Chemical composition, oxygen impurity content, density, mean grain size and microhardness of sintered materials. The relative density has been estimated from the density of the starting materials.

	Composition (wt.%)	Oxygen impurity (%.wt)	Density (g/cm^3)	Relative density (%)	Grain Size (µm)	Micro-hardness (MPa)
C-Cu1Y	1 Y	0.017	8.41 ±0.02	95	20 ±4	680 ±40
PM-Cu1Y	1 Y	0.016	9.08 ±0.02	99	8 ±2	712 ±20
PM-Cu1Y_2O_3	1 Y_2O_3	0.038	8.78 ±0.02	102	16 ±3	620 ±30

Table 2: Most characteristic tensile properties for Cu1Y tested at a strain rate of 1.1×10^{-4} s^{-1}.

Temp (K)	Yield Strength (MPa)	Ultimate Tensile Strength (UTS) (MPa)	Maximum Plastic Strain (%)	Hardening ratio UTS/YS
293	135 ± 14	320 ± 12	26 ± 3	2.4 ± 0.3
373	128 ± 13	280 ± 7	19 ± 3	2.2 ± 0.3
473	125 ± 6	236 ± 9	20 ± 3	1.89 ± 0.16
573	111 ± 5	166 ± 6	11 ± 2	1.49 ± 0.12
673	97 ± 3	129 ± 4	10.5 ± 1.4	1.33 ± 0.12
773	79 ± 4	93 ± 3	9.9 ± 0.8	1.18 ± 0.10

Figure captions:

Fig. 1: Optical a) and SEM-BSE images b) of C-Cu1Y. Inset in b) shows the formation of microcraks in yttrium-enriched regions. c) EDS spectra of different regions: (—), (-□-) and (-Δ-) correspond to spectra collected from regions 1, 2, and 3 respectively. (-○-) displays the spectrum inside a Cu grain (region 4). EDS spectra have been normalized to equal area over the measured energy range.

Fig.2: XRD patterns of the produced materials: a) vacuum induction melting C-Cu1Y, (b) PM-Cu1Y cryomilled powder and HIP sintered material and (c) PM-CuY_2O_3 milled powder and HIP sintered material.

Fig. 3: Optical a) and TEM b) images of PM-Cu1Y. Inset (SEM-BSE) shows yttrium-rich oxides (dark contrast) decorating the grain boundaries.

Fig. 4: Optical a) and TEM b) images of PM-CuY_2O_3. Inset in a) (SEM-SE image) shows yttrium-rich oxides (bright contrast) decorating grain boundaries. Inset in b) shows an Y_2O_3 particle in the copper matrix.

Fig. 5: Tensile stress-strain curves as a function of the temperature for PM-Cu1Y (strain rate 1.1×10^{-4} s^{-1}). The inset depicts the 0.02% Yield Strength (YS-□) and the Ultimate Tensile Strength (UTS-●) as a function of the temperature.

Fig. 6: SEM images of the fracture surface of PM-Cu1Y at RT (a) SEM-SE and (b) SEM-BSE images, and at 573 K (c) SEM-SE and (d) SEM-BSE images. Light-gray contrast on images (b) and (c) corresponds with yttrium-rich oxide particles.